

Communication

Dual-Response Photofunctional Covalent Organic Framework for Acid Detection in Various Solutions

Wenyue Ma ¹, Zijian Gu ¹, Guocui Pan ¹, Chunjuan Li ², Yu Zhu ², Zhaoyang Liu ¹, Leijing Liu ¹, Yupeng Guo ², Bin Xu ¹ and Wenjing Tian ^{1,*}¹ State Key Laboratory of Supramolecular Structure and Materials, College of Chemistry, Jilin University, Changchun 130012, China² National Chemistry Experimental Teaching Demonstration Center, Jilin University, Changchun 130012, China

* Correspondence: wjtian@jlu.edu.cn

Abstract: The detection of acid in different solution environments plays a significant role in chemical, environmental and biological fields. However, reducing the constraints of detecting environment, such as aqueous, organic solvents and mixed phases of aqueous and organic phases, remains a challenge. Herein, by combining N, N, N', N'-tetrakis(4-aminophenyl)-1,4-phenylenediamine (TPBD) and terephthalaldehyde (TA) via Schiff-base condensation, we constructed a covalent organic framework (COF) TPBD-TA COF. The COF exhibits color change from red to dark red as well as fluorescence quenching with the increase of acid contents in either aqueous or organic solvents, or a mixture of aqueous and organic solvents, due to the weak donor-acceptor interactions within the COF as well as the weak proton ionization ability of the solutions. Therefore, regardless of the detection environment, TPBD-TA COF can realize color and fluorescence dual-response to acid with the detection limit as low as 0.4 $\mu\text{mol/L}$ and 58 nmol/L , respectively, due to the protonation of the nitrogen atoms on imine bonds of the COF.

Keywords: covalent organic framework; color change; fluorescence quenching; acid detection



Citation: Ma, W.; Gu, Z.; Pan, G.; Li, C.; Zhu, Y.; Liu, Z.; Liu, L.; Guo, Y.; Xu, B.; Tian, W. Dual-Response Photofunctional Covalent Organic Framework for Acid Detection in Various Solutions. *Chemosensors* **2023**, *11*, 214. <https://doi.org/10.3390/chemosensors11040214>

Academic Editor: Jose V. Ros-Lis

Received: 3 March 2023

Revised: 18 March 2023

Accepted: 28 March 2023

Published: 30 March 2023



Copyright: © 2023 by the authors. Licensee MDPI, Basel, Switzerland. This article is an open access article distributed under the terms and conditions of the Creative Commons Attribution (CC BY) license (<https://creativecommons.org/licenses/by/4.0/>).

1. Introduction

Covalent organic frameworks (COFs), two-dimensional [1–7] or three-dimensional [8–11] crystalline porous organic polymers, constructed by organic building blocks through covalent bonds [12–17] have been applied in energy storage [18,19], gas adsorption and separation [20,21], catalysis [22], chemical separation [23,24] and optoelectronics [25,26] due to their controllable structure, easy functionalization, excellent crystallinity and porosity [27,28]. The ordered channels formed by periodic pores of COFs provide more space for host-guest molecules to interact with each other, which is beneficial for sensing and detecting. Acid detection in solution plays an important part in environmental surveillance, water quality, chemical reaction control and medical diagnosis [29]. Photofunctional materials, especially COFs, play a significant role in the field of detection [30–32]. Using COFs as chemosensors to detect acid in solution via colorimetric and fluorescence methods with the advantage of the high sensitivity, fast response and easy operation has already achieved significant progress. For example, Liu et al. constructed the first fluorescent pH sensor COF-JLU4 [33] to detect pH in aqueous solution. Wang and his co-workers prepared COF-HQ, whose emission intensity and colour were sensitive to pH in aqueous solution [34]. Auras et al. synthesized star-shaped dual-pore perylene-based 2D COFs and realized acid vapor detection in nonaqueous solution [35]. Gao et al. achieved the reversible color and fluorescent response of VCOF-PyrBpy to acids/pH in water [36]. The above examples show color switching or/and fluorescence decreasing response to acid in either aqueous or nonaqueous solutions. However, it is generally difficult to realize acid detection in different kinds of solutions (aqueous solution, organic solvents and mixture of aqueous and organic solvents) simultaneously. This is because H^+ from different solvents will interact with

the frameworks weakly or strongly, resulting in more or less protonation to change the intramolecular electronic transitions of the frameworks, and further causing the change of photophysical properties of the COFs [29,36].

In fact, the protonation of the linkage or linker of COFs will cause the intraframework charge transfer or change the π -electron conjugation of the framework, thereby altering the photophysical properties of the COFs; as such, the COFs can be used as chemosensors for acid detecting. In order to realize acid detection in different kinds of solutions, selecting the structure of COFs with weak donor-acceptor charge transfer interactions is anticipated. In this case, different solvents will not induce the obvious charge transfer effect of the COFs, thereby breaking the detection environmental limitations for acid detection.

Herein, we use N, N, N', N'-tetrakis(4-aminophenyl)-1,4-phenylenediamine (TPBD) with rich nitrogen atoms and terephthalaldehyde (TA) to prepare photofunctional TPBD-TA COF through Schiff-base reaction. The COF exhibits obvious absorption red-shifts in UV-vis spectra and the fluorescence intensity of the COF decreases with increasing acid concentration in different kinds of solution (aqueous solutions, organic solvents and mixed solution of aqueous and organic phases) due to the protonation of nitrogen atoms on imine bonds. Thus, TPBD-TA COF, which exhibits weak donor-acceptor interactions, can serve as a versatile chemosensor for detecting acid in different solutions.

2. Materials and Methods

2.1. Materials and Instrumentations

N, N, N', N'-tetrakis(4-aminophenyl)-1,4-phenylenediamine (TPBD) and terephthalaldehyde (TA) were purchased from Leyan. o-Dichlorobenzene, n-BuOH, acetone, tetrahydrofuran (THF), ethanol (EtOH), acetonitrile (MeCN), methanol (MeOH), toluene, HCl, trifluoroacetic acid (TFA), trifluoromethanesulfonic acid (TFMS), 4-methylbenzenesulfonic acid (TsOH) and benzaldehyde were purchased from Titan.

The solid-state ^{13}C cross-polarization/magic-angle spinning (CP/MAS) NMR spectra were collected using a Bruker AVANCE III 400 WB spectrometer. The time-of-flight mass spectra were recorded using a Kratos MALDI-TOF mass system (Bruker, Billerica, MA, USA). Fourier transform infrared (FT-IR) spectra were recorded on a Vertex 80 V spectrometer (Bruker, Rosenheim, Germany). The sample was grinded into powder and dried, then mixed with dried KBr (powder) and pressed into piece. UV-Vis spectra were recorded with a Shimadzu UV-2550 spectrophotometer (Tokyo, Japan). Fluorescence spectroscopy was taken using a Shimadzu RF-5301 PC spectrometer. SEM images were recorded using scanning electron microscopy (Hitachi Regulus 8100, Hitachi, Japan). A drop of the aqueous solution was dripped directly onto a silicon wafer and air-dried. The TEM image was recorded using a JEM-2100F instrument (JEOL Ltd., Beijing, China) with an accelerating voltage of 200 kV. The sample was prepared by placing a drop of the stock solution on a 300-mesh, carbon-coated copper grid and air-dried before measurement. The N_2 adsorption-desorption isotherms were measured using a Quantachrome Autosorb-iQ2 analyzer (Boynton Beach, FL, USA). Powder X-ray diffraction (PXRD) was performed with a Rigaku D/MAX2550 diffractometer (Rigaku, Tokyo, Japan) using $\text{Cu-K}\alpha$ radiation, 40 kV, 200 mA at room temperature.

2.2. The Solid-State UV-Vis Absorption Test of TPBD-TA COF on Detecting Acid

TPBD-TA COF was dispersed in aqueous solution, organic solvents and mixed solutions of aqueous and organic solvents with different amounts of acid, then the COF powder was filtered. The filtered powder was used to perform solid-state absorption spectrum tests.

2.3. The Fluorescence Test of TPBD-TA COF on Detecting Acid

TPBD-TA COF was dispersed in aqueous solution, organic solvents and mixed solutions of aqueous and organic solvents, then certain concentrations of the acid were gradually added to the COF suspension. The COF suspension (0.5 mg mL^{-1}) with different concentrations of acid was used to perform fluorescence tests.

2.4. The Recyclability Test of the COF

The PL spectra of TPBD-TA COF in ethanol solution and after adding TFA were recorded. Then, we washed the COF with water until the pH of the solvent was 7 and then dried the COF at 120 °C under vacuum for 4 h for the measurement of PXRD of the COF. The COF was used to detect acid for next cycle by repeating the above processes.

2.5. The Preparation of COF Filter Paper

Polystyrene (PS) (300 mg) was dissolved in toluene (2 mL) by stirring overnight. Then, TPBD-TA COF (10 mg) suspension (2 mL) was added into the toluene solution of PS and stirred at room temperature for several hours. The mixed solution was filtrated on the filter paper, thereby forming the COF filter paper.

3. Results and Discussion

3.1. Synthesis and Characterization

TPBD-TA COF (Figure S1) was synthesized by using N, N, N', N'-tetrakis (4-aminophenyl)-1,4-phenylenediamine (TPBD) as the knot and terephthalaldehyde (TA) as the linker through Schiff-base reaction [37]. The COF were characterized by powder X-ray diffraction (PXRD), Fourier transform infrared spectroscopy (FT-IR), solid state ¹³C CP/ MAS NMR, thermogravimetric analysis (TGA), field transmission electron microscopy (TEM) and scanning electron microscopy (SEM).

FT-IR spectra (Figure S3a) and solid-state ¹³C CPMAS NMR spectra (Figure S3b) of TPBD-TA COF confirmed the formation of imine bonds (at 1621 cm⁻¹ and 156 ppm, respectively). PXRD measurement (Figure S3c) indicated the crystallinity of the COF. As shown in Figure S3c, the PXRD profile of TPBD-TA COF displays a series of reflection peaks at 2.47°, 4.45°, 4.49°, 6.49°, 8.93° and 21.13°, which can be assigned to (100), (110), (200), (210), (310) and (001) facets of TPBD-TA COF, respectively. The (001) plane at 21.13° is attributed to π - π stacking between the adjacent layers of the COF. In order to investigate the structure and stacking mode of the COF, theoretical simulations were carried out using Materials Studio software packages. Pawley refinements with the unit cell (P-3, a = b = 43.35 Å and c = 4.46 Å) producing the Pawley-refined pattern of TPBD-TA COF matched well with the experimental results (Rwp = 7.7%). By comparing the PXRD patterns of the simulated TPBD-TA COF with the experimental pattern (red curve), it is indicated that the COFs adopt the eclipsed AA-stacking mode instead of the staggered AB-stacking mode. The porosity of the COF was proved by nitrogen adsorption measurements at 77 K. In Figure S3d, a steep N₂ adsorption at low relative pressure indicates that the COF has micropores; in addition, there was a hysteresis loop in the degassing process, showing that the COF has mesopores. The Brunauer–Emmett–Teller (BET) surface area was calculated to be 510.2 m²g⁻¹. The pore size distribution was at 1.73 and 2.94 nm, calculated by using nonlocal density functional theory (NLDFT). The TEM image (Figure S4a) showed that TPBD-TA COF manifested a layered stacking structure. The SEM image (Figure S4b) revealed the COF was microparticles with sheet-like morphologies. In the TGA experiment (Figure S5), the COF exhibited slight weight loss at about 450 °C under an N₂ atmosphere, suggesting high thermostability. To investigate the chemical stability of the COF, we measured XRD (Figure S6) of the COF immersed in different solvents for 2 days at room temperature. There was a slight change of the PXRD curves of the COF immersed in different solvents for 48 h when compared with the original (black curve); however, the crystallinity of the COF immersed in different solvents was still retained, indicating the excellent chemical stability of TPBD-TA COF.

We investigated the photophysical properties of TPBD-TA COF by recording UV-vis absorption spectra and fluorescence emission spectra. The COF was dispersed in various solvents, such as acetone, tetrahydrofuran (THF), ethanol (EtOH), acetonitrile (MeCN), methanol (MeOH) and H₂O; we then filtered the powders to perform solid-state UV-vis absorption tests. As shown in Figure S7, the absorption bands of the COF showed slight red- or blue-shift with the increase of the solvent polarity, and the fluorescence spectra of

the suspension in acetone, THF, EtOH, MeCN, MeOH and H₂O featured emission peaks at 623, 633, 635, 624, 637 and 629 nm, respectively (Figure S8); this means that there is no obvious solvatochromic behavior for the COF in solvents with different polarity since the weak donor-acceptor structure of TPBD-TA COF will not induce apparent intraframework charge transfer by increasing the polarity of solvents.

3.2. Acid Sensing

Supported by the chemical stability and photophysical properties of TPBD-TA COF, we investigated the acid-response properties of the COF in various solutions via UV–Vis absorption and fluorescence spectra.

As shown in Figure 1b, the absorption spectra of TPBD-TA COF in HCl aqueous solution displayed a gradual increase in the new absorption bands at the range from 600 nm to 850 nm when the concentration of HCl in water increased from 0 μ M to 16.67 μ M. Similarly, the new absorption band emerged with the increasing concentration of TFA in water (Figure S9a). The response of TPBD-TA COF to inorganic acid (HCl) and organic acid (TFA) in water solution illustrates that COF can detect different kinds of acid in aqueous solution. When TsOH, an organic acid, was dispersed in MeCN, the absorption bands of TPBD-TA COF gradually shifted towards longer wavelengths as the concentration of TsOH increased (Figure S9b). When the COF was scattered in MeOH and the concentration of TFA increased from 0 mM to 0.5 mM, the additional absorption band of the COF gradually emerged in the range from 600 nm to 840 nm (Figure S9c). The response of TPBD-TA COF to TsOH and TFA in organic solvents demonstrates that COF can detect organic acid in different organic solvents. The reason for the response of TPBD-TA COF to inorganic and organic acids is that H⁺ from acid can protonate nitrogen atoms on imine bonds of the COF (Figure 1a); this will increase the donor-acceptor interaction between TPBD and TA moiety of the protonated COF, leading to the red-shifted absorption upon successive adding of H⁺. Therefore, TPBD-TA COF can be used as an acidochromism sensor to detect both inorganic and organic acid in aqueous solutions as well as organic acid in organic solvents.

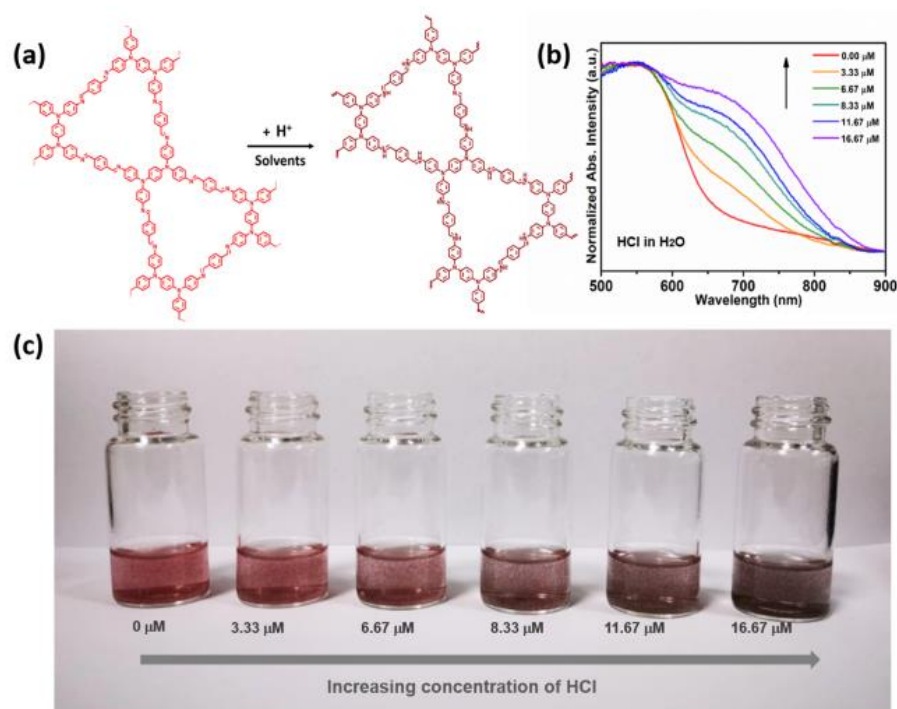


Figure 1. (a) Protonation process of TPBD-TA COF in acidic solutions, (b) solid-state absorption spectra of TPBD-TA COF in HCl aqueous solution, (c) color change of TPBD-TA COF in HCl aqueous solution with increased HCl concentration.

A pronounced color change of the COF from red to dark red (Figure 1c and Figure S10) was observed when the COF powders were immersed in various solutions with different contents of acid.

We attempted to calculate the detection limit of the acid-responsive COF. The relationship between the absorbance change or fluorescence sensing response and acid concentration was explored using the following equations [38,39]: $\Delta A = 1 + K[C]$ (1), $I_0/I = 1 + K[C]$ (2), where ΔA was the absorbance change of the COF before and after acid addition; I_0 was the initial luminescent intensity of the COF suspensions without acid; I was the luminescent intensity of the COF suspensions with different contents of acid; K was the absorbance change constant or the quenching constant; and $[C]$ was the concentration of acid. Then we calculated the limit of detection (LOD) using the following formula [40,41]: $LOD = 3S/K$ (3), where S was the standard deviation of the absorption or fluorescence response for TPBD-TA COF without adding acid and K was the absorbance change constant or the quenching constant. Therefore, the LOD values for the COF detecting HCl in H_2O , TFA in H_2O , TsOH in MeCN and TFA in MeOH were $0.4 \mu\text{mol L}^{-1}$, $14.7 \mu\text{mol L}^{-1}$, $3.26 \mu\text{mol L}^{-1}$ and $26.7 \mu\text{mol L}^{-1}$, respectively.

Figure 2 illustrates the change in fluorescence intensity of TPBD-TA COF in response to different acid solutions with varying acid concentrations, as well as the corresponding LOD values. As shown in Figure 2a, with the addition of HCl in aqueous solution, the fluorescence intensity of the COF decreases gradually. The change in the fluorescence intensity maintains a good linear fit with the acid concentrations (Figure 2b), to give an accurate LOD value. Meanwhile, the fluorescence of the COF can be also quenched by TFA in aqueous solution (Figure S11a), indicating that the COF can detect acid in water. As revealed in Figure S11b, when TPBD-TA COF was dispersed in an MeCN solution of TsOH, the fluorescence intensity of the COF can be obviously attenuated with the increase of acid concentration from $0 \mu\text{M}$ to $60 \mu\text{M}$. Similarly, the fluorescence intensity of TPBD-TA COF suspension was quenched by increasing the concentration of TFA in MeOH (Figure S11c). This fluorescence quenching is attributed to the protonated nitrogen atoms on imine bonds, which destroy the π -electron-conjugated system of TPBD-TA COF upon acid addition [42].

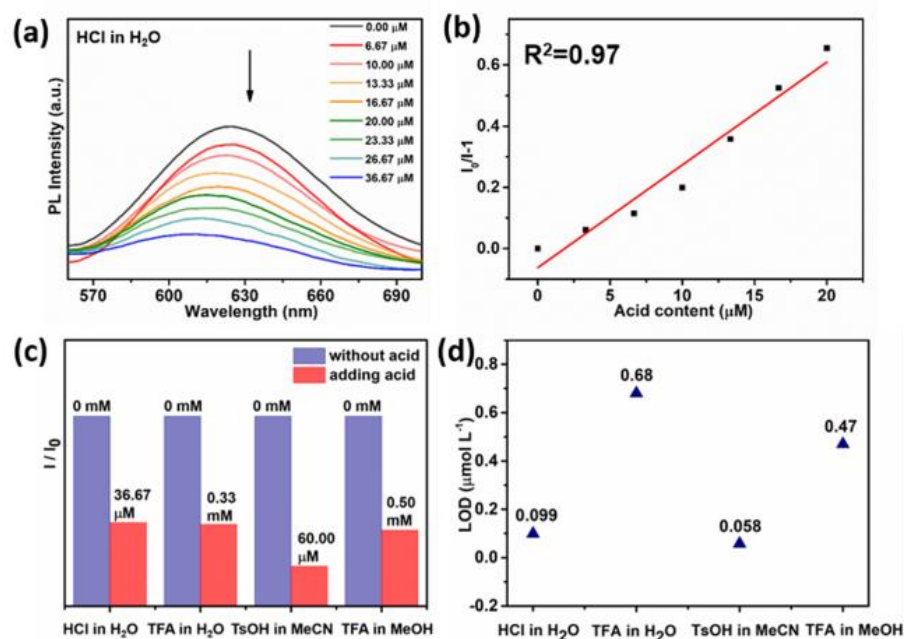


Figure 2. (a) Fluorescence spectra of TPBD-TA COF in HCl aqueous solution with different acid concentration ($\lambda_{\text{ex}} = 365 \text{ nm}$), (b) the linear relationship between acid content and emission ratios, (c) emission ratio before and after adding acid, (d) the LOD values of detecting different acid in different solutions.

It can be seen from Figure 2c that the COF can detect inorganic acid in aqueous solutions and organic acid in either aqueous solutions or organic solvents via fluorescence approaches with the detection limit of $0.099 \mu\text{mol L}^{-1}$, $0.68 \mu\text{mol L}^{-1}$, $0.058 \mu\text{mol L}^{-1}$ and $0.47 \mu\text{mol L}^{-1}$ for detecting HCl in H_2O , TFA in H_2O , TsOH in MeCN and TFA in MeOH (Figure 2d), respectively.

The detection ability of the COF toward acid in the mixture of aqueous solution and organic solvents was further explored by UV–Vis absorption and fluorescence spectra (Figure 3). As shown in Figure 3a, when the COF was immersed in EtOH solution of TFA with 5% water, an additional absorption band in the range of 600–800 nm and a red-shift of the absorption band was observed as the acid concentration increased. When the water content increased to 10%, 20%, 40%, 60% and 80%, the absorption bands of the COF were red-shifted gradually to 800 nm (Figures S12a–d and 3b). The red-shifted absorption of the COF is attributed to the interaction between H^+ from acid and nitrogen atoms of imine bonds of the COF. Of course, different kinds of solvents also released H^+ , but it is difficult to induce apparent intraframework charge transfer effects within the COF with weak donor–acceptor interaction because the concentration of H^+ ionized from solvents is very low. The COF exhibits excellent linear relationships between the absorption change and the acid content (Figure 3e). The detection limit of the COF to detect TFA in mixed solutions of EtOH and H_2O was in the range of $0.059 \text{ mmol L}^{-1} \sim 0.24 \text{ mmol L}^{-1}$ (Figure 3f).

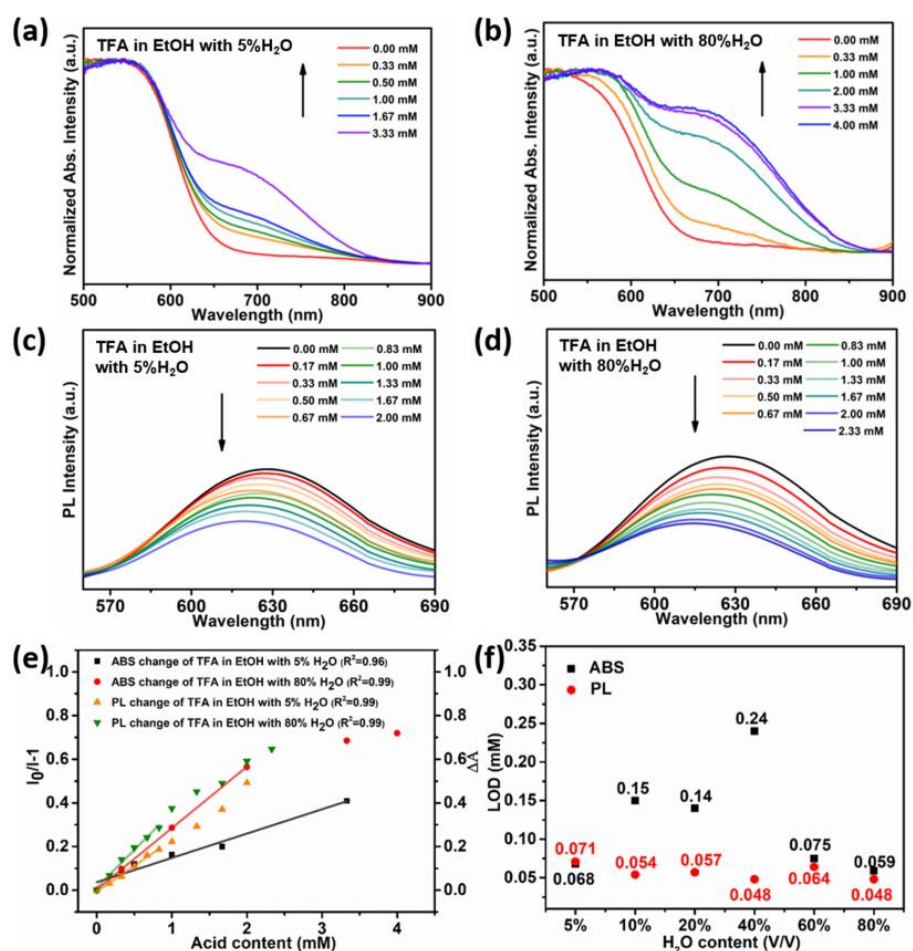


Figure 3. Solid-state absorption spectra of TPBD-TA COF in EtOH solutions of TFA with (a) 5% water, (b) 80% water (V/V) and different acid concentration, fluorescence spectra of TPBD-TA COF in TFA EtOH solution with (c) 5% water, (d) 80% water (V/V) and different acid concentration, (e) the linear relationship between acid content and emission ratios/or absorption change, (f) the LOD values of detecting TFA in EtOH solutions with different amount of water.

The acid response of the COF to TFA in acetone aqueous solution (Figure S13), TsOH in MeCN aqueous solution (Figure S14) and trifluoromethanesulfonic acid (TFMS) in EtOH aqueous solution (Figure S15) indicates that TPBD-TA COF can be used as a colorimetric sensor to detect acid in different solutions with the LOD ranging from $0.9 \mu\text{mol L}^{-1}$ to 0.22 mmol L^{-1} .

The fluorescence spectra of TPBD-TA COF in EtOH solution of TFA with different water (V/V; 5%, 10%, 20%, 40%, 60% and 80%) and different acid concentrations are shown in Figures 3c,d and S16. These spectra indicate that no matter the amount of water in ethanol, the fluorescence intensity of the COF is significantly correlated with the acid content, i.e., the fluorescence intensity gradually decreases with the increase of the acid concentration. In addition, the COF exhibits a good linear relationship between the emission ratio and the acid content (Figure 3e). The LOD value was as low as $0.048 \text{ mmol L}^{-1}$ (Figure 3f). The fluorescence quenching effect of the COF was demonstrated in the mixed solutions of water and organic solvents when increasing the acid concentration of TFA, TsOH and TFMS (Figures S17–S19). Because the protonating ability of H^+ from solvents to nitrogen atoms on imine bonds is weaker than that of H^+ from acid, the solvents hardly lead to the change of π -electron-conjugated system of the COF, thereby facilitating the detection of acid in different kinds of solution by the COF.

To evaluate the recyclability of TPBD-TA COF as a fluorescent sensor to probe acid, we recorded acid-dependent fluorescence spectra for five continuous cycles (Figure S20). The fluorescence was quenched after acid was added, and the color of the COF quickly turned from red to dark red. The emission can return to similar intensities and the color of the COF can convert back to red after removing acid from the suspension of the COF through water washing. Moreover, the crystallinity of the COF remained after five cycles (Figure S21), demonstrating the responsive reproducibility of TPBD-TA COF to acid.

3.3. Acid Sensing Mechanism

In order to prove the protonated site of the COF, we synthesized the model compound (1) and tested absorption and fluorescence responses of TPBD and the model compound to acid, respectively. As shown in Figure S22a, the absorption intensity of TPBD gradually increases and the absorption bands display an obvious blue-shift with increasing acid concentration; this is different from the appearance of a new absorption peak of the COF with the increased acid concentration, illustrating that the acidochromism of the COF does not originate from the protonation of the free amine. In Figure S22b, a new absorption band of the model compound gradually emerged from 450 nm to 600 nm as a result of increasing acid concentration; this is consistent with the acidochromism of the COF, which proves the acidochromism of the COF is from the protonation of the imine nitrogen of the COF. In Figure S22c, the fluorescence intensity of TPBD first decreased and then increased with the increase of acid concentration; this is different from the gradually decreased fluorescence intensity of the COF with the increase of the acid concentration, indicating the fluorescence quenching of the COF is not attributed to the protonation of the free amine. Furthermore, the fluorescence intensity of the model compound gradually decreases when the acid concentration increases (Figure S22d). This is consistent with the response of the COF to acid, illustrating that the emission quenching comes from protonation of imine nitrogen of the COF.

In order to further investigate the acid sensing mechanism of the COF, we calculated the electronic cloud distribution of the COF before and after protonation by using Density functional theory (DFT). Before the addition of acid, partly separation of the electronic cloud density between the highest occupied molecular orbital (HOMO) and the lowest unoccupied molecular orbital (LUMO) can be observed, where the electronic cloud of the HOMO was distributed on TPBD and benzene of TA (Figure S23a); meanwhile, the electron cloud of the LUMO was primarily distributed on TA (Figure S23b). It means that the COF had a weak intramolecular charge transfer (ICT) property before protonation, which is consistent with the photophysical property (Figures S7 and S8). After the addition of acid,

the nitrogen atoms in imine bonds of the COF were protonated, leading to well-separated electronic cloud density between HOMO and LUMO. As revealed in Figure S23c,d, the electronic cloud distribution on HOMO was dominated by TPBD units, while that on LUMO was dominated by TA units, indicating the formation of charge transfer (CT) state from TPBD moiety to TA moiety with the increase of acid concentration. Compared with the non-protonated imine, the protonated imine of the COF is a stronger acceptor, leading to a lower bandgap from 1.27 eV to 0.70 eV, as well as red-shifted absorption. That is why we can observe color change of the COF from red to dark red when increasing the acidity.

As shown in Figure S23, when compared with the deprotonated COF, the electron cloud density distribution of the protonated COF has smaller π -electron-conjugated range. The damaged π -electron-conjugated system of the COF by the protonation of acid is the reason for the fluorescence quenching. Meanwhile, the weak H^+ ionization ability of solvent can hardly change the π -electron-conjugated system of the COF and the dipole strength of donor-acceptor pair neither. This is to say that the solvent has little effect on acid-response fluorescence of the COF. Therefore, TPBD-TA COF can be applied as a fluorescent acid sensor to detect acid in different solvents via fluorescence method.

In order to further investigate the acid sensing mechanism of the COF, we calculated the natural transition orbitals (NTOs) of the deprotonated COF and the protonated COF (Figure S23e). The holes of the deprotonated COF were distributed on TPBD and TA moieties, while the electrons were distributed on TA moiety; this indicates that the deprotonated COF had some charge transfer property in the excited state. However, when the COF was protonated, the holes were distributed on TPBD unit and the electrons were primarily distributed on the TA moiety, predicting the obvious charge transfer property of the protonated COF in the excited state. However, the weak transition oscillator strength ($f = 0.0870$) led to a low probability of the ICT process, resulting in fluorescence quenching of the protonated COF.

The electronic cloud distributions of the COF in different solvents (acetone, ethanol and H_2O) were calculated using DFT to prove that different solvents had little effect on them. As shown in Figure S24a, the electronic cloud between HOMO and LUMO of the COF in acetone was partly overlapped, illustrating the weak intramolecular charge transfer interaction within the COF. Meanwhile, the electronic cloud distributions of the COF in ethanol (Figure S24b) and H_2O (Figure S24c) were the same as that in acetone. Moreover, the electronic cloud distributions of the COF in different kinds of solvents with different polarity were similar to that of the COF without solvent (Figure S23a), providing more evidence to prove that the solvents had almost no influence on photophysical properties of the COF. It endows good properties of TPBD-TA COF in detecting acid in various solutions.

3.4. Acid Sensing Application

The acid detection test paper was prepared by using TPBD-TA COF to detect different kinds of acids in varied solutions. As revealed in Figure 4a, when different solvents were dropped on the papers, there was no color change. However, when different solvents with acid were dropped on the test paper, the color of the paper immediately change from red to dark-red (Figure 4a).

The acid-responsive properties of TPBD-TA COF endow it with significant application potential in information encryption. When we wrote a Chinese knot pattern on the COF filter paper using TFA in EtOH solution, the dark-red Chinese knot pattern was observed, as shown in Figure 4b. Then, the COF filter paper was exposed to NH_3 (20–28%) vapor and the pattern vanished (encrypt information). After the filter paper was heated for about two minutes, the dark-red Chinese knot pattern appeared on the paper again. This process could be repeated at least four times, demonstrating the potential application of the COF in the field of information encryption.

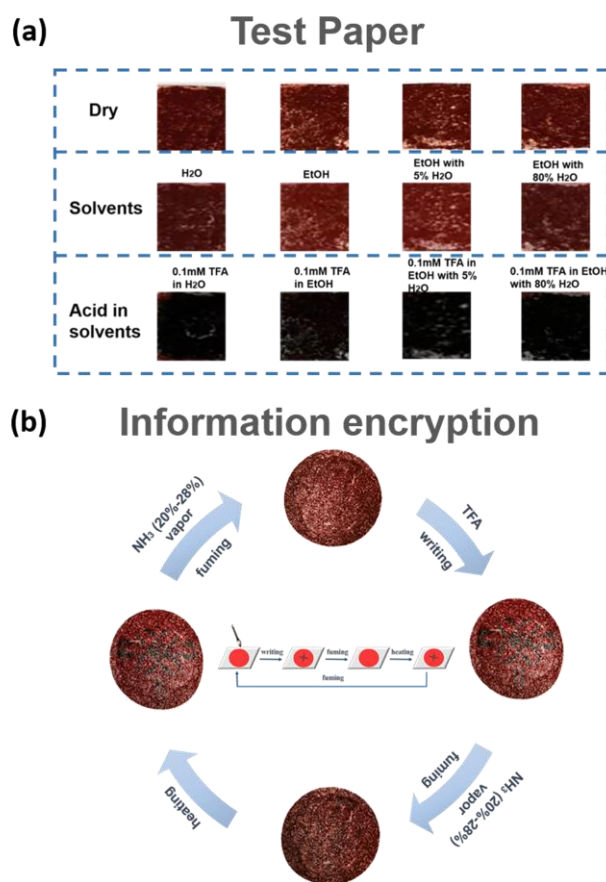


Figure 4. (a) Changes in color of TPBD-TA COF-based test paper before and after dropping solvents and acidic solutions, (b) visible picture of TPBD-TA COF filter paper through 0.1 mM TFA writing and NH₃ (20–28% aqueous solution) vapor erasing.

4. Conclusions

In summary, we have synthesized a dual-mode acid sensing photofunctional COF through Schiff-base reaction that can detect acid in aqueous solutions, organic solvents and mixed solutions of aqueous and organic solvents due to the weak donor-acceptor interactions within the COF and the weak proton ionization ability of the solvents. The COF shows obvious color change from red to dark red as acid concentration increases in different solutions with a good detecting level (LOD = 0.4 $\mu\text{mol L}^{-1}$). In addition, different concentrations of acid in various kinds of solvents can also cause the decreased fluorescence intensity of TPBD-TA COF; the LOD value is as low as 0.058 $\mu\text{mol L}^{-1}$. TPBD-TA COF breaks the constraints of the detecting environment; this endows it with significant prospects in future applications for detecting acid in various solutions.

Supplementary Materials: The following supporting information [37,43,44] can be downloaded at: <https://www.mdpi.com/article/10.3390/chemosensors11040214/s1>.

Author Contributions: Conceptualization, methodology, software, validation and writing—original draft preparation, W.M.; data curation, Z.G.; theoretical calculation, G.P.; experimental treatment, C.L. and Y.Z.; polish manuscript, Z.L. and L.L.; instrument support, Y.G.; funding acquisition, B.X. and W.T. All authors have read and agreed to the published version of the manuscript.

Funding: This work was supported by the National Natural Science Foundation of China (21835001, 52073116, 21674041, 51773080) and the JLU Science and Technology Innovative Research Team (2021TD-03).

Institutional Review Board Statement: Not applicable.

Informed Consent Statement: Not applicable.

Data Availability Statement: Not available.

Conflicts of Interest: The authors declare no conflict of interest.

References

1. Jiang, S.; Meng, L.C.; Ma, W.Y.; Pan, G.C.; Zhang, W.; Zou, Y.C.; Liu, L.J.; Xu, B.; Tian, W.J. Dual-functional two-dimensional covalent organic frameworks for water sensing and harvesting. *Mater. Chem. Front.* **2021**, *5*, 4193–4201. [[CrossRef](#)]
2. Wang, P.; Xu, Q.; Li, Z.P.; Jiang, W.M.; Jiang, Q.H.; Jiang, D.L. Exceptional Iodine Capture in 2D Covalent Organic Frameworks. *Adv. Mater.* **2018**, *30*, 1801991. [[CrossRef](#)] [[PubMed](#)]
3. Spitler, E.L.; Koo, B.T.; Novotney, J.L.; Colson, J.W.; Uribe-Romo, F.J.; Gutierrez, G.D.; Clancy, P.; Dichtel, W.R. A 2D Covalent Organic Framework with 4.7-nm Pores and Insight into Its Interlayer Stacking. *J. Am. Chem. Soc.* **2011**, *133*, 19416–19421. [[CrossRef](#)] [[PubMed](#)]
4. Colson, J.W.; Woll, A.R.; Mukherjee, A.; Levendorf, M.P.; Spitler, E.L.; Shields, V.B.; Spencer, M.G.; Park, J.; Dichtel, W.R. Oriented 2D Covalent Organic Framework Thin Films on Single-Layer Graphene. *Science* **2011**, *332*, 228–231. [[CrossRef](#)]
5. Evans, A.M.; Parent, L.R.; Flanders, N.C.; Bisbey, R.P.; Vitaku, E.; Kirschner, M.S.; Schaller, R.D.; Chen, L.X.; Gianneschi, N.C.; Dichtel, W.R. Seeded growth of single-crystal two-dimensional covalent organic frameworks. *Science* **2018**, *361*, 53–57. [[CrossRef](#)]
6. Mohamed, M.G.; Lee, C.C.; El-Mahdy, A.F.M.; Luder, J.; Yu, M.H.; Li, Z.; Zhu, Z.L.; Chueh, C.C.; Kuo, S.W. Exploitation of two-dimensional conjugated covalent organic frameworks based on tetraphenylethylene with bicarbazole and pyrene units and applications in perovskite solar cells. *J. Mater. Chem. A* **2020**, *8*, 11448–11459. [[CrossRef](#)]
7. Lv, Y.K.; Li, Y.S.; Zhang, G.; Peng, Z.X.; Ye, L.; Chen, Y.; Zhang, T.; Xing, G.L.; Chen, L. An In Situ Film to Film Transformation Approach toward Highly Crystalline Covalent Organic Framework Films. *Ccs Chem.* **2022**, *4*, 1519–1525. [[CrossRef](#)]
8. Fang, Q.R.; Gu, S.; Zheng, J.; Zhuang, Z.B.; Qiu, S.L.; Yan, Y.S. 3D Microporous Base-Functionalized Covalent Organic Frameworks for Size-Selective Catalysis. *Angew. Chem. Int. Edit.* **2014**, *53*, 2878–2882. [[CrossRef](#)]
9. Lin, G.Q.; Ding, H.M.; Chen, R.F.; Peng, Z.K.; Wang, B.S.; Wang, C. 3D Porphyrin-Based Covalent Organic Frameworks. *J. Am. Chem. Soc.* **2017**, *139*, 8705–8709. [[CrossRef](#)]
10. El-Kaderi, H.M.; Hunt, J.R.; Mendoza-Cortes, J.L.; Cote, A.P.; Taylor, R.E.; O’Keeffe, M.; Yaghi, O.M. Designed synthesis of 3D covalent organic frameworks. *Science* **2007**, *316*, 268–272. [[CrossRef](#)]
11. Zhu, Q.; Wang, X.; Clowes, R.; Cui, P.; Chen, L.J.; Little, M.A.; Cooper, A.I. 3D Cage COFs: A Dynamic Three-Dimensional Covalent Organic Framework with High-Connectivity Organic Cage Nodes. *J. Am. Chem. Soc.* **2020**, *142*, 16842–16848. [[CrossRef](#)]
12. Cote, A.P.; Benin, A.I.; Ockwig, N.W.; O’Keeffe, M.; Matzger, A.J.; Yaghi, O.M. Porous, crystalline, covalent organic frameworks. *Science* **2005**, *310*, 1166–1170. [[CrossRef](#)] [[PubMed](#)]
13. Hunt, J.R.; Doonan, C.J.; LeVangie, J.D.; Cote, A.P.; Yaghi, O.M. Reticular synthesis of covalent organic borosilicate frameworks. *J. Am. Chem. Soc.* **2008**, *130*, 11872–11873. [[CrossRef](#)] [[PubMed](#)]
14. Li, Y.S.; Chen, W.B.; Xing, G.L.; Jiang, D.L.; Chen, L. New synthetic strategies toward covalent organic frameworks. *Chem. Soc. Rev.* **2020**, *49*, 2852–2868. [[CrossRef](#)] [[PubMed](#)]
15. Rodriguez-San-Miguel, D.; Montoro, C.; Zamora, F. Covalent organic framework nanosheets: Preparation, properties and applications. *Chem. Soc. Rev.* **2020**, *49*, 2291–2302. [[CrossRef](#)] [[PubMed](#)]
16. Segura, J.L.; Mancheno, M.J.; Zamora, F. Covalent organic frameworks based on Schiff-base chemistry: Synthesis, properties and potential applications. *Chem. Soc. Rev.* **2016**, *45*, 5635–5671. [[CrossRef](#)]
17. Huang, N.; Wang, P.; Jiang, D.L. Covalent organic frameworks: A materials platform for structural and functional designs. *Nat. Rev. Mater.* **2016**, *1*, 1–19. [[CrossRef](#)]
18. Hu, Y.M.; Dunlap, N.; Wan, S.; Lu, S.L.; Huang, S.F.; Sellinger, I.; Ortiz, M.; Jin, Y.H.; Lee, S.H.; Zhang, W. Crystalline Lithium Imidazolate Covalent Organic Frameworks with High Li-Ion Conductivity. *J. Am. Chem. Soc.* **2019**, *141*, 7518–7525. [[CrossRef](#)]
19. Mohamed, M.G.; Atayde, E.C.; Matsagar, B.M.; Na, J.; Yamauchi, Y.; Wu, K.C.W.; Kuo, S.W. Construction Hierarchically Mesoporous/Microporous Materials Based on Block Copolymer and Covalent Organic Framework. *J. Taiwan Inst. Chem. Eng.* **2020**, *112*, 180–192. [[CrossRef](#)]
20. Shan, M.X.; Liu, X.L.; Wang, X.R.; Yarulina, I.; Seoane, B.; Kapteijn, F.; Gascon, J. Facile manufacture of porous organic framework membranes for precombustion CO₂ capture. *Sci. Adv.* **2018**, *4*, eaau1698. [[CrossRef](#)]
21. Khan, N.A.; Zhang, R.N.; Wu, H.; Shen, J.L.; Yuan, J.Q.; Fan, C.Y.; Cao, L.; Olson, M.A.; Jiang, Z.Y. Solid-Vapor Interface Engineered Covalent Organic Framework Membranes for Molecular Separation. *J. Am. Chem. Soc.* **2020**, *142*, 13450–13458. [[CrossRef](#)] [[PubMed](#)]
22. Ren, X.M.; Li, C.Z.; Kang, W.C.; Li, H.; Ta, N.; Ye, S.; Hu, L.Y.; Wang, X.L.; Li, C.; Yang, Q.H. Enormous Promotion of Photocatalytic Activity through the Use of Near-Single Layer Covalent Organic Frameworks. *CCS Chem.* **2022**, *4*, 2429–2439. [[CrossRef](#)]
23. Kang, Z.X.; Peng, Y.W.; Qian, Y.H.; Yuan, D.Q.; Addicoat, M.A.; Heine, T.; Hu, Z.G.; Tee, L.; Guo, Z.G.; Zhao, D. Mixed Matrix Membranes (MMMs) Comprising Exfoliated 2D Covalent Organic Frameworks (COFs) for Efficient CO₂ Separation. *Chem. Mater.* **2016**, *28*, 1277–1285. [[CrossRef](#)]
24. Fan, H.W.; Mundstock, A.; Feldhoff, A.; Knebel, A.; Gu, J.H.; Meng, H.; Caro, J. Covalent Organic Framework-Covalent Organic Framework Bilayer Membranes for Highly Selective Gas Separation. *J. Am. Chem. Soc.* **2018**, *140*, 10094–10098. [[CrossRef](#)] [[PubMed](#)]

25. Rice, A.M.; Dolgoplova, E.A.; Yarbrough, B.J.; Leith, G.A.; Martin, C.R.; Stephenson, K.S.; Heugh, R.A.; Brandt, A.J.; Chen, D.A.; Karakalos, S.G.; et al. Stack the Bowls: Tailoring the Electronic Structure of Corannulene-Integrated Crystalline Materials. *Angew. Chem. Int. Edit.* **2018**, *57*, 11310–11315. [[CrossRef](#)]
26. Zhang, L.; Yi, L.; Sun, Z.J.; Deng, H.X. Covalent organic frameworks for optical applications. *Aggregate* **2021**, *2*, 13011. [[CrossRef](#)]
27. Diercks, C.S.; Yaghi, O.M. The atom, the molecule, and the covalent organic framework. *Science* **2017**, *355*, eaal1585. [[CrossRef](#)]
28. Feng, L.; Wang, K.Y.; Day, G.S.; Zhou, H.C. The chemistry of multi-component and hierarchical framework compounds. *Chem. Soc. Rev.* **2019**, *48*, 4823–4853. [[CrossRef](#)]
29. Gilmanova, L.; Bon, V.; Shupletsov, L.; Pohl, D.; Rauche, M.; Brunner, E.; Kaskel, S. Chemically Stable Carbazole-Based Imine Covalent Organic Frameworks with Acidochromic Response for Humidity Control Applications. *J. Am. Chem. Soc.* **2021**, *143*, 18368–18373. [[CrossRef](#)]
30. Luo, Y.C.; Zhang, S.; Wang, H.; Luo, Q.; Xie, Z.G.; Xu, B.; Tian, W.J. Precise Detection and Visualization of Cyclooxygenase-2 for Golgi Imaging by a Light-Up Aggregation-Induced Emission Based Probe. *CCS Chem.* **2022**, *4*, 456–463. [[CrossRef](#)]
31. Meng, L.C.; Ma, X.B.; Jiang, S.; Zhang, S.; Wu, Z.Y.; Xu, B.; Lei, Z.; Liu, L.J.; Tian, W.J. Twisted Intramolecular Charge Transfer-Aggregation-Induced Emission Fluorogen with Polymer Encapsulation-Enhanced Near-Infrared Emission for Bioimaging. *CCS Chem.* **2021**, *3*, 2084–2094. [[CrossRef](#)]
32. Wu, Z.Y.; Zhang, C.Y.; Zhu, Y.L.; Lu, Z.Y.; Liu, H.; Xu, B.; Zhang, X.Q.; Tian, W.J. Visualization of Macrophase Separation and Transformation in Immiscible Polymer Blends. *Ccs Chem.* **2022**, *2022*, 1–11. [[CrossRef](#)]
33. Zhang, Y.W.; Shen, X.C.; Feng, X.; Xia, H.; Mu, Y.; Liu, X.M. Covalent organic frameworks as pH responsive signaling scaffolds. *Chem. Commun.* **2016**, *52*, 11088–11091. [[CrossRef](#)] [[PubMed](#)]
34. Long, C.; He, L.W.; Ma, F.Y.; Wei, L.; Wang, Y.X.; Silver, M.A.; Chen, L.H.; Lin, Z.; Gui, D.X.; Juan, D.W.; et al. Covalent Organic Framework Functionalized with 8-Hydroxyquinoline as a Dual-Mode Fluorescent and Colorimetric pH Sensor. *ACS Appl. Mater. Inter.* **2018**, *10*, 15364–15368.
35. Ascherl, L.; Evans, E.W.; Gorman, J.; Orsborne, S.; Bessinger, D.; Bein, T.; Friend, R.H.; Auras, F. Perylene-Based Covalent Organic Frameworks for Acid Vapor Sensing. *J. Am. Chem. Soc.* **2019**, *141*, 15693–15699. [[CrossRef](#)]
36. Bu, R.; Zhang, L.; Liu, X.Y.; Yang, S.L.; Li, G.; Gao, E.Q. Synthesis and Acid-Responsive Properties of a Highly Porous Vinylene-Linked Covalent Organic Framework. *ACS Appl. Mater. Inter.* **2021**, *13*, 26431–26440. [[CrossRef](#)]
37. Hao, Q.; Li, Z.J.; Bai, B.; Zhang, X.; Zhong, Y.W.; Wan, L.J.; Wang, D. A Covalent Organic Framework Film for Three-State Near-Infrared Electrochromism and a Molecular Logic Gate. *Angew. Chem. Int. Edit.* **2021**, *60*, 12498–12503. [[CrossRef](#)]
38. Sung, T.W.; Lo, Y.L. Ammonia vapor sensor based on CdSe/SiO₂ core-shell nanoparticles embedded in sol-gel matrix. *Sens. Actuat. B Chem.* **2013**, *188*, 702–708. [[CrossRef](#)]
39. Wang, Y.F.; Liu, X.; Wang, M.K.; Wang, X.X.; Ma, W.Y.; Li, J.Y. Facile synthesis of CDs@ZIF-8 nanocomposites as excellent peroxidase mimics for colorimetric detection of H₂O₂ and glutathione. *Sens. Actuat. B Chem.* **2021**, *329*, 129115. [[CrossRef](#)]
40. Balaji, T.; Sasidharan, M.; Matsunaga, H. Optical sensor for the visual detection of mercury using mesoporous silica anchoring porphyrin moiety. *Analyst* **2005**, *130*, 1162–1167. [[CrossRef](#)]
41. Richardson, T.H.; Dooling, C.M.; Jones, L.T.; Brook, R.A. Development and optimization of porphyrin gas sensing LB films. *Adv. Colloid Interface Sci.* **2005**, *116*, 81–96. [[CrossRef](#)] [[PubMed](#)]
42. Jiang, H.L.; Feng, D.W.; Wang, K.C.; Gu, Z.Y.; Wei, Z.W.; Chen, Y.P.; Zhou, H.C. An Exceptionally Stable, Porphyrinic Zr Metal-Organic Framework Exhibiting pH-Dependent Fluorescence. *J. Am. Chem. Soc.* **2013**, *135*, 13934–13938. [[CrossRef](#)] [[PubMed](#)]
43. Grigoras, M.; Stafie, L. Synthesis and Characterization of Linear, Branched and Hyperbranched Triphenylamine-Based Polya-zomethines. *Des. Monomers Polym.* **2009**, *12*, 177–196. [[CrossRef](#)]
44. Frisch, M.J.; Trucks, G.W.; Schlegel, H.B.; Scuseria, G.E.; Robb, M.A.; Cheeseman, J.R.; Scalmani, G.; Barone, V.; Mennucci, B.; Petersson, G.A.; et al. *Gaussian 09, Revision D.01*; Gaussian, Inc.: Wallingford, CT, USA, 2009.

Disclaimer/Publisher's Note: The statements, opinions and data contained in all publications are solely those of the individual author(s) and contributor(s) and not of MDPI and/or the editor(s). MDPI and/or the editor(s) disclaim responsibility for any injury to people or property resulting from any ideas, methods, instructions or products referred to in the content.